



Synthesis and Electrochemical Characteristics of Spherical $\text{Li}_4\text{Ti}_5\text{O}_{12}$ /CNT Composite Materials for Hybrid Capacitors

Joeng-Jin Yang^{1,3}, Yu-Ri Kim¹, Moon-Gook Jeong³, Yong-Jae Yuk², Han-Joo Kim², and Soo-Gil Park^{1*}

¹Department of Industrial Engineering Chemistry, Chungbuk National University

²PureEChem Co., Ltd., Cheongju Chungbuk Korea

³Waseda University, Shinjuku Japan

ABSTRACT

Spherical $\text{Li}_4\text{Ti}_5\text{O}_{12}$ and $\text{Li}_4\text{Ti}_5\text{O}_{12}$ carbon nanotube (CNT) composites were synthesized using a colloid system. The electrochemical properties of the composites were thoroughly examined to determine their applicability as hybrid capacitor anodes. The electrical conductivity of the spherical $\text{Li}_4\text{Ti}_5\text{O}_{12}$ -CNT composite was improved over that of the spherical $\text{Li}_4\text{Ti}_5\text{O}_{12}$ composite. The synthesized composites were utilized as the anode of a hybrid capacitor, which was assembled with an activated carbon (AC) positive electrode. The CNTs attached on the spherical $\text{Li}_4\text{Ti}_5\text{O}_{12}$ particles contributed to a 51% reduction of the equivalent series resistance of the $\text{Li}_4\text{Ti}_5\text{O}_{12}$ -CNTs/AC hybrid capacitor compared to the $\text{Li}_4\text{Ti}_5\text{O}_{12}$ /AC hybrid capacitor. Moreover, the $\text{Li}_4\text{Ti}_5\text{O}_{12}$ -CNTs/AC hybrid capacitor showed a larger capacitance than the $\text{Li}_4\text{Ti}_5\text{O}_{12}$ /AC hybrid capacitor; specifically, the $\text{Li}_4\text{Ti}_5\text{O}_{12}$ -CNT/AC hybrid capacitor showed 1.6 times greater capacitance at 40 cycles with a 10 mA cm^{-2} loading current density.

Keywords: Spherical $\text{Li}_4\text{Ti}_5\text{O}_{12}$, $\text{Li}_4\text{Ti}_5\text{O}_{12}$ -CNT composite, $\text{Li}_4\text{Ti}_5\text{O}_{12}$ /AC hybrid capacitors

Received May 8, 2015 : Accepted June 1, 2015

1. Introduction

Studies on environmentally friendly energy production systems have recently emerged owing to concerns about environmental pollution, global warming, and fossil fuel depletion. In addition, the smart grid system has been commercialized by improving the production efficiency, transmission, and distribution of electric power. Moreover, energy storage devices have been developed for smart grid applications. In general, energy storage systems are classified in two types: high power storage devices and small-to-medium portable energy storage devices [1-3]. Lith-

ium ion secondary batteries (LIBs) are considered small-to-medium energy storage devices. However, in spite of the high energy density of LIBs, their low power density is problematic when they are operated with high current. Electrochemical capacitors (ECs), on the other hand, can be utilized under high current owing to their high power density; however, they have a low energy density.

The mechanism of ECs is determined only by the physical adsorption of ions on the surface of the active materials, which can realize the high power density [1]. To enhance the low energy density of ECs, hybrid systems have been developed that take

*Corresponding author. Tel.: +82-43-261-2492, Fax: +82-43-273-8221

E-mail address: sgpark@cbnu.ac.kr

Open Access DOI: <http://dx.doi.org/10.5229/JECST.2015.6.2.59>

This is an Open Access article distributed under the terms of the Creative Commons Attribution Non-Commercial License (<http://creativecommons.org/licenses/by-nc/3.0/>) which permits unrestricted non-commercial use, distribution, and reproduction in any medium, provided the original work is properly cited.

advantage of the LIB redox reaction [4-5]. The resulting hybrid systems, or hybrid capacitors (HCs), are determined from the different electrochemical mechanisms arising in the cathode and anode as well as by the active materials composing each electrode. For example, the electrodes of HCs are assembled using LIB cathodes such as lithium manganese oxide (LMO) [6-8] with EC anodes such as activated carbon (AC); conversely, HCs could be assembled using LIB anodes such as lithium titanium oxide (LTO) [9,10] or graphite [11,12] with EC cathodes such as AC. As a result, the hybrid system can enhance the energy density with twice the capacitance of electric double-layer capacitors (EDLCs) [13]. However, when metal oxides are used for the cathode or anode material, the internal resistance is increased, resulting in a reduced power density [14]. Therefore, the synthesis of carbon and metal oxide composite materials has been studied to prevent the increase in internal resistance. For example, carbon composite hybrid systems, which are composites containing carbon nanotubes (CNTs) [15,16], graphene [17], or activated carbon [18], have been considered. Moreover, carbon coating could be applied to the surface of the metal oxide using carbonization [19].

In this study, we prepared $\text{Li}_4\text{Ti}_5\text{O}_{12}$ -CNT composite materials synthesized by the sol-gel process to enhance of power density of $\text{Li}_4\text{Ti}_5\text{O}_{12}$, which is used as a negative active material that has a zero-strain behavior and high charge-discharge performance [20]. Then, the electrochemical characteristics of the $\text{Li}_4\text{Ti}_5\text{O}_{12}$ -CNT composite HC anode were examined and compared to those of the $\text{Li}_4\text{Ti}_5\text{O}_{12}$ HC anode.

2. Experimental

2-1. Synthesis and analysis of LTO and LTO-CNT composite materials

To synthesize LTO-CNT, 0.1 g of hydro-propyl cellulose (HPC, Sigma-Aldrich) was dissolved into n-octanol (99%, Samchun) followed by dispersion in titanium isopropoxide (TTIP, Sigma-Aldrich) [21]. The CNTs were pretreated by stirring in 0.1-M nitric acid for 1 h. The CNTs were then washed in distilled water and dried at 80°C. The CNTs were added into the TTIP dispersant solution at 1, 2, and 3 wt.% of the amount of synthesized LTO and were dispersed using a homogenizer (T-25 Digital Ultra-Turrax, Ika). Then, the colloid was formed by adding acetonitrile

(99.8%, Sigma-Aldrich) with an agitation speed of 12000 rev min⁻¹. Lithium hydroxide (LiOH, Sigma-Aldrich) solution was added into the formed colloid for the sol-gel reaction process and was stirred with an agitation speed of 12000 rev min⁻¹. After the sol-gel reaction was completed, the solvent and reactant of the colloid solution were separated using a centrifuge operating at 1000 rev min⁻¹. The reactant was rinsed three times with ethanol followed by drying at 60°C using an oven. After the reactant was completely dried, the reactant was calcinated for 5 h under N₂ atmosphere. The morphological characteristics of the synthesized LTO-CNT composites were observed by field-emission scanning electron microscope (FE-SEM, LEO-1530), and the crystal structure analysis was performed by X-ray diffraction (XRD, XDS2000).

2-2. Electrode preparation and electrochemical characterization

The synthesized LTO-CNT was casted on Al foil (20-μm thickness) to explore the electrochemical characteristics for comparison with the LTO composite. The LTO-CNT electrode was prepared by blending calcinated LTO-CNT powder (88 wt.%), carbon black (10 wt.%), and binder (5 wt.%), which consisted of carboxymethyl cellulose (CMC, 1 wt.%, Sigma-Aldrich), styrene butadiene rubber (SBR, 2 wt.%, Sigma-Aldrich), polytetrafluoro-ethylene (PTFE, 2 wt.%, Sigma-Aldrich), with distilled water. The thickness was controlled mass of double by the relative mass of the LTO and LTO-CNT composite electrodes. For electrochemical characterization, a two-electrode system was assembled using the LTO and LTO-CNT composite as a working electrode, a Li disk as a counter-electrode, and 1 M of LiBF_4 in propylene carbonate as an electrolyte.

A can-type HC was assembled with a size of $\Phi 10 \times L 20$ mm. The positive and negative electrodes were 123 mm \times 14 mm and 139 mm \times 14 mm, respectively, and lead taps were attached on each electrode. The two electrodes were placed face-to-face and dried in a vacuum oven at 120°C for 12 h. For assembling the three-electrode system, the Li disk was used as a reference electrode, and 1 M of LiBF_4 in propylene carbonate was used as an electrolyte. Moreover, the electrochemical impedance spectroscopy (EIS) was measured from 100 kHz to 10 mHz with an amplitude of 10 mV at open circuit voltage.

3. Results and Discussion

Fig. 1 shows the FE-SEM images of the LTO and LTO-CNT composites synthesized by colloidal synthesis. The colloid was formed in water/oil (W/O) biphases, which contain n-Octanol as the oil phase and acetonitrile as the water phase. Spherical LTO was synthesized via substitution reaction of TTIP, which was homogeneously dispersed in the oil phase, when water was added to the colloid mixture. The colloid formed spheres in the mixing solution. The reaction continuously occurred because acetonitrile absorbed the water, causing solidification of the precursor. Moreover, Li was homogeneously dispersed in the TiO_2 particles using aqueous LiOH. Figs. 1(a-d) show the SEM images of LTO, LTO-CNT 1%, LTO-CNT 2%, and LTO-CNT 3%, respectively, with the high magnification images provided in the inset. The SEM results indicated that spherical particles with size of approximately $20\ \mu\text{m}$ were synthesized. The surface of the raw LTO was assumed to be aggregated with the unit crystal structure; otherwise, the LTO surface may have cracked owing to growth of the unit crystal structure during the calcination process. The LTO particles containing CNTs showed irregular morphologies owing to the attached CNTs on the LTO surface, which significantly changed as the CNT amount increased. During the colloidal process, the CNT additive hindered the preparation of spherical col-

loids because the CNTs acted as an impurity, disturbing the formation of a stable water–oil interface. Thus, the colloid of LTO-CNT composite materials could not form spherical particles when more than 3 wt.% CNTs were added, as shown in Fig. 1(d).

The crystal structure of the synthesized LTO and LTO-CNT composite was analyzed using XRD, as shown in Fig. 2. Peaks at $2\theta = 18.3^\circ$, 43.3° , and 35.6° , which were respectively assigned to (111), (400), and (311) of the LTO crystal structure, were clearly obtained. The diffraction patterns of the synthesized LTO and LTO-CNT composite were in agreement with the structure of $\text{Li}_{1.33}\text{Ti}_{1.66}\text{O}_4$ (JCPDS no. 26-1198). The electrochemical impedance spectra of the LTO and LTO-CNT composite were investigated and compared to determine the change in resistance caused by the CNT composite.

Fig. 3 shows the EIS results with the typical Randles circuit. In typical EIS, the equivalent series of resistance (ESR) is obtained at the high frequency region followed by charge transfer resistance (R_{ct}) at the high-to-mid frequency region. The suppressed semi-circle with the LTO composite had a larger magnitude compared to that of the LTO-CNT composite, which implies that R_{ct} was reduced. The CNT additives enhanced the electrical conductivity by forming a conductive network that improved the effective electron path. However, the charge transfer resistance did not continuously decrease with the increasing CNT content because the CNTs only influenced the electron path. The CNTs are unrelated to the reaction of Li^+ . In high frequencies, the resistance value of ESR also decreased with increasing additive CNTs. The raw LTO materials had an ESR value of

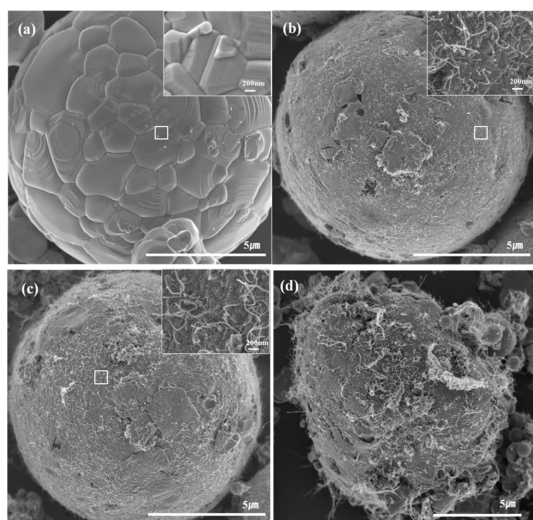


Fig. 1. The FE-SEM images of the (a) LTO, (b) LTO-CNT 1 wt.%, (c) LTO-CNT 2 wt.%, and (d) LTO-CNT 3 wt.% particles.

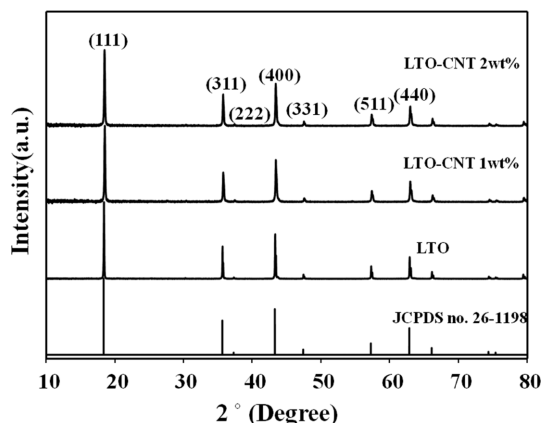


Fig. 2. The XRD patterns for LTO and LTO-CNT composite materials.

about $9.9\ \Omega$ while that of LTO-CNT 1 wt.% and LTO-CNT 2 wt.% was $8.8\ \Omega$ and $8.5\ \Omega$, respectively.

Figs. 4(a-c) show the charge-discharge profiles of

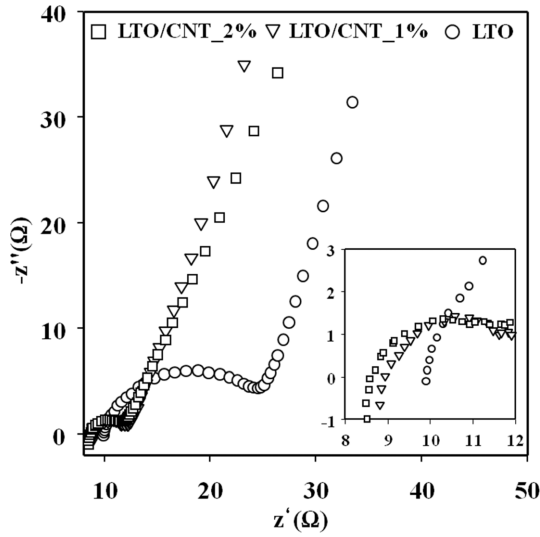


Fig. 3. Electrochemical impedance spectroscopy of LTO and LTO-CNT composite materials from 100 kHz to 10 mHz with an amplitude of 10 mV at open circuit voltage.

the synthesized materials, while Fig. 4(d) shows the C-rate characteristics of the synthesized materials with increasing cycle number. The LTO materials have a three-electron redox reaction in the range of 1.45 V–1.75 V (vs. Li/Li^+) due to Ti^{3+} and Ti^{4+} , which has a known theoretical capacity of about $175\ \text{mAh g}^{-1}$. The redox reaction in the range of 1.45–1.75 V (vs. Li/Li^+) is shown by a horizontal line. In Fig. 4(a-c), the constant value around 1.6 V (vs. Li/Li^+) indicates the stable redox reaction of Ti^{3+} and Ti^{4+} . The synthesized LTO material capacities were measured at about $131.9\ \text{mAh g}^{-1}$, which is about 75.4% of the theoretical capacity. The decreased capacity is related to the surface of the LTO materials, which are likely rock-stone by calcination, as shown in Fig. 1. The non-activated volume inside the LTO materials further influenced the capacity. The initial capacities of the LTO materials were larger than those of the LTO-CNT composite materials because of the CNT content. Fig. 4(d) shows the C-rate characteristics with respect to the additive CNTs. When the CNT weight ratio increases, the capacities increase. For example, the capacity of LTO is $56.6\ \text{mAh g}^{-1}$, while the capacity of LTO-CNT 1 wt.% is $75.8\ \text{mAh g}^{-1}$ and that of LTO-CNT 2 wt.% is $91.2\ \text{mAh g}^{-1}$. As a result, the

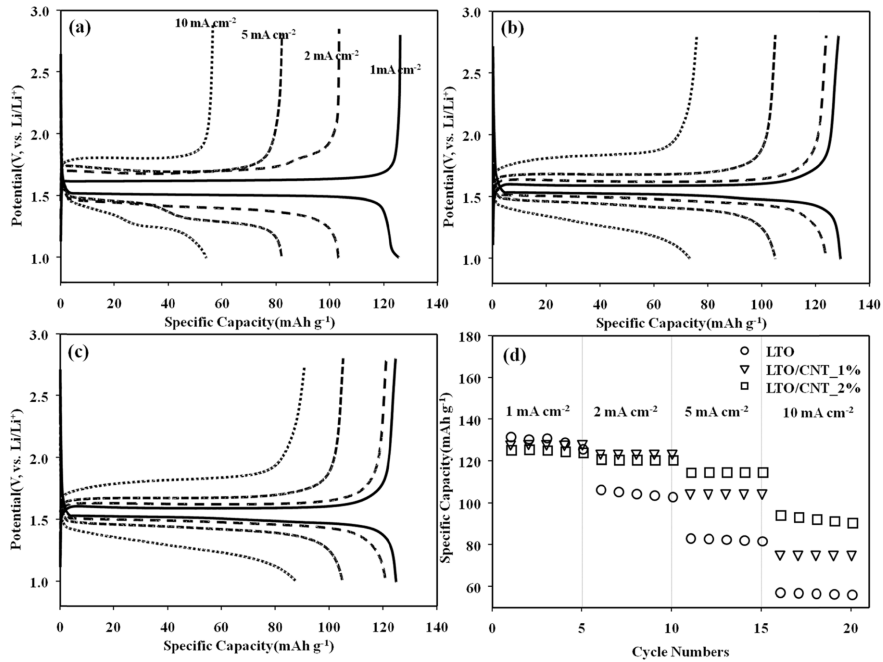


Fig. 4. Potential profiles of (a) LTO, (b) LTO-CNT 1 wt.%, and (c) LTO-CNT 2 wt.%. (d) The C-rate characteristics of samples with various current densities.

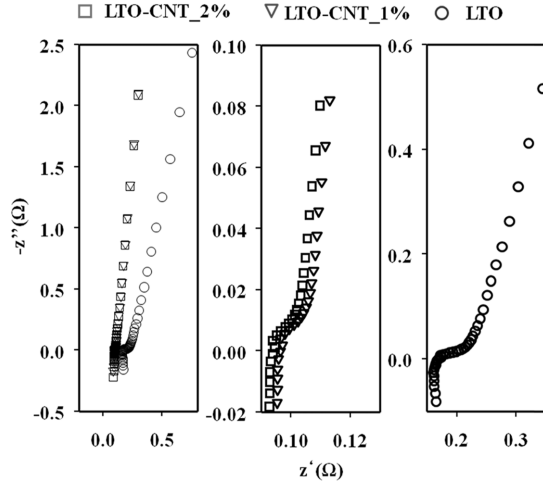


Fig. 5. Electrochemical impedance spectroscopy of LTO-AC, LTO-CNT 1 wt.%/AC, and LTO-CNT 2 wt.%/AC hybrid capacitors from 100 kHz to 10 mHz with an amplitude of 10 mV at open circuit voltage.

additive CNTs influenced the C-rate characteristics because of the decreasing electric conductivity.

Fig. 5 shows the electrochemical impedance spectra of the hybrid capacitors, which are assembled with an AC positive electrode and LTO or LTO-CNT composite negative electrode. The ESR values of the LTO/AC, LTO-CNT 1 wt.%/AC, and LTO-CNT 2 wt.%/AC hybrid capacitors are confirmed to be about 192.7, 102.3, and 99.3 mΩ, respectively, at 1 kHz. Moreover, in low frequencies, the EIS characteristics are similar to electric double-layer capacitance; specifically, when the surface of the electrode is fully charged, the impedance is shown by a vertical line in the z - z graph. The characteristics of decreasing ESR in hybrid capacitors are attributed to the additive CNTs. As shown Fig. 3, additive CNTs influence the ESR of hybrid capacitors.

Figs. 6(a-c) show the charge-discharge profile of the LTO/AC hybrid capacitor, LTO-CNT 1 wt.%/AC

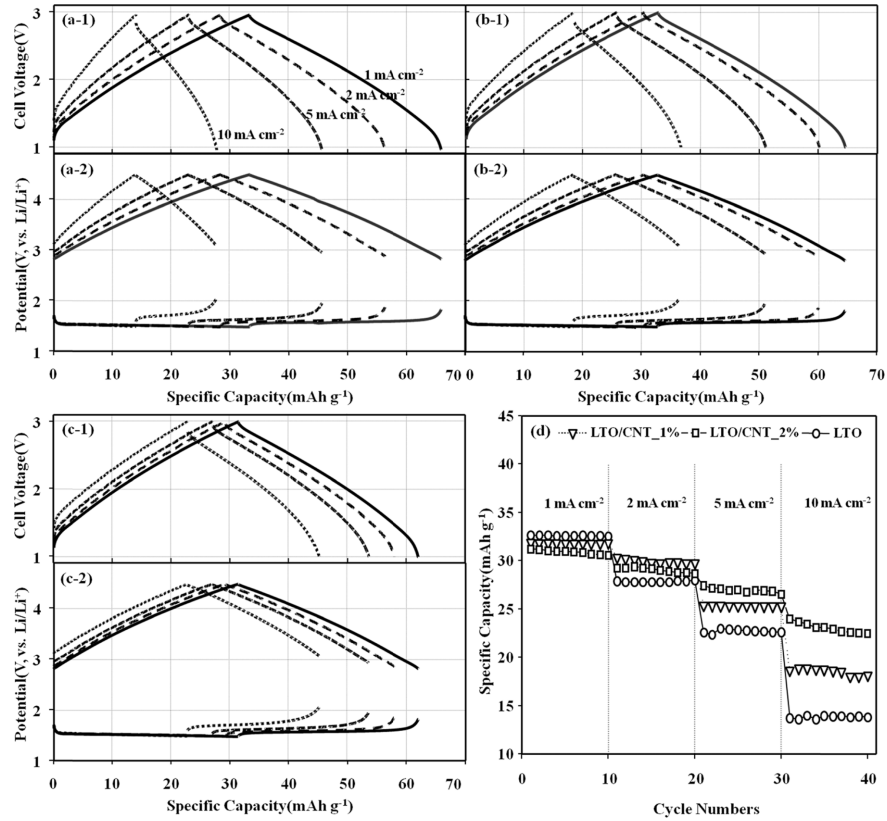


Fig. 6. Voltage profiles of (a-1) LTO/AC, (b-1) LTO-CNT 1 wt.%/AC, and (c-1) LTO-CNT 2 wt.%/AC hybrid capacitors. (a-2), (b-2), and (c-2) show the potential profiles of the negative and positive electrodes in the respective hybrid capacitors with various current densities. (d) The C-rate characteristics of the hybrid capacitors.

hybrid capacitor, and LTO-CNT 2 wt.%/AC hybrid capacitor, respectively. Specifically, Fig. 6(a-1), (b-1), and (c-1) are the voltage profiles of the hybrid capacitors, while Fig. 6(a-2), (b-2), and (c-2) are the voltage profiles of the positive and negative electrodes in the hybrid capacitors. When the voltage of hybrid capacitors ranged from 1 V to 3 V, the positive electrode operated from about 2.8 V to 4.48 V (vs. Li/Li⁺), while the negative electrode operated from about 1.8 V to 1.47 V (vs. Li/Li⁺). The operating potentials of the positive and negative electrode are observed to have a similar voltage range. In low current densities, the characteristics attributed to the mass ratio of the negative electrode to the positive electrode (N/P mass ratio) of the hybrid capacitor and the LTO and LTO-CNT composite materials have similar capacities. As shown in Fig. 6(d), at 40 cycles, the capacity of the LTO material was about 42% of that in the first cycle in 10 mA cm⁻². However, the LTO-CNT 1 wt.% and LTO-CNT 2 wt.% composite materials maintained about 57% and 72% of the original capacity, respectively. The remaining capacities of the LTO and LTO-CNT composite materials show the power density. As a result, the additive CNTs influence the power density because of their enhanced conductivity. When applied in hybrid systems as electrochemical capacitors, the high capacities of LTO materials influence the enhancement of the energy density in hybrid capacitors. The resulting capacity is twice that of commercial EDLCs.

4. Conclusion

Hybrid capacitors are developed using LTO as a negative electrode material and AC as a positive electrode material. The spherical LTO materials were synthesized in a colloidal system using a sol-gel process. During the synthesis, CNTs were added in varying amounts from 1 wt.% to 3 wt.%. The electrochemical characteristics of the synthesized LTO and LTO-CNT composites were measured by EIS and by charge-discharge tests. The charge transfer resistance and ESR of LTO materials were confirmed to decrease as the CNT content increased. When applied in a hybrid capacitor, we confirmed the decreasing ESR of the hybrid capacitor. Thus, the LTO-CNT 1 wt.% and LTO-CNT 2 wt.% hybrid capacitors had capacities that were 31.6% and 62.7% larger than that of the LTO-AC hybrid capacitor, respectively, in a current density of 10 mA cm⁻² at 40 cycles. In conclusion, the addition of CNTs improved the hybrid capacitor because of the electron path formation in LTO materials.

Acknowledgement

This work was supported by the Human Resource Training Program for Regional Innovation through the Ministry of Education and National Research Foundation of Korea (NRF-2012H1B8A2025592) and Technical Innovation and Development Project of small and medium business administration.

Reference

- [1] B.E. Conway, *Electrochemical Supercapacitor-Scientific Fundamentals and Technological Application*, Kluwer Academic, New York (1999).
- [2] M. Winter and R.J. Brodd, *Cehm. Rev.* **104**, 4245 (2004).
- [3] M. Inagaki, H. Konno, and O. Tanaike, *J. Power sources*, **195**, 7880 (2010).
- [4] S. Nomoto, H. Nakata, K. Yoshioka, A. Yoshida, and H. Yoneda, *J. Power Sources*, **97-98**, 807 (2001).
- [5] D. Cericola and R. Kotz, *Electrochim. Acta*, **72**, 1 (2012).
- [6] M.S. Hong, S.H. Lee, and S.W. Kim, *Electrochem. Solid-state Lett.*, **5**, A227 (2002).
- [7] M.Y. Cho, S.M. Park, J.W. Lee, and K.C. Roh, *J. Electrochem. Sci. Technol.*, **2**(3), 152 (2011).
- [8] H.U. Kim, K.H. Shin, B.S. Lee, M.S. Jeon, K.N. Jung, Y.K. Sun, and C.S. Jin, *J. Electrochem. Sci. Technol.*, **1**(2), 97 (2010).
- [9] X.B. Hu, Y.J. Huai, Z.J. Lin, J.S. Suo, and Z.H. Deng, *J. Electrochem. Soc.*, **154**, A1026 (2007).
- [10] H. S. Choi, J. H. Im, T.H. Kim, J.H. Park, and C.R. Park, *J. Mater. Chem.*, **22**, 16986 (2012).
- [11] J.H. Lee, W.H. Shin, M.H. Ryou, J.K. Jin, J. Kim, and J.W. Choi, *ChemSusChem*, **5**(12), 2328 (2012).
- [12] S.R. Sivakkumar and A.G. Pandolfo, *Electrochim. Acta*, **65**, 280 (2012).
- [13] J.J. Yang, C.H. Choi, H.B. Seo, H.J. Kim, and S.G. Park, *Electrochim. Acta*, **86**, 277 (2012).
- [14] P.V. Braun, J. Cho, J.H. Pikul, W.P. King, and H. Zhang, *Curr. Opin. Solid State Mater. Sci.*, **16**, 186 (2012).
- [15] X. Li, M. Qu, Y.J. Huai, and Z. Yu, *Electrochim. Acta*, **55**, 2978 (2010).
- [16] H.I. Kim, J.J. Yang, H.J. Kim, T. Osaka, and S.G. Park, *Korean Electrochem. Soc.*, **13**(4), 235 (2010).
- [17] L. Ye, Q. Liang, Y. Lei, X. Yu, C. Han, W. Shen, Z.H. Huang, F. Kang, and Q.H. Yang, *J. Power sources*, **282**, 174 (2015).
- [18] J.J. Yang, H.I. Kim, Y.J. Yuk, H.J. Kim, and S.G. Park, *J. Electrochem. Sci. Technol.*, **1**(1), 63 (2010).
- [19] H.G. Jung, N. Venugopal, B. Scrosati, and Y.K. Sun, *J. Power sources*, **221**, 266 (2013).
- [20] T.F. Yi, L.J. Jiang, J. Shu, C.B. Yue, R.S. Zhu, and H.B. Qiao, *J. Phys. Chem. Solids*, **71**, 1236 (2010).
- [21] S.L. Chou, J.Z. Wang, H.K. Liu, and S.X. Dou, *J. Phys. Chem. C*, **115**, 16220 (2011).